SIAM J. SCI. COMPUT.
Vol. 41, No. 1, pp. B139–B152

SHARP QUADRATURE ERROR BOUNDS FOR THE NEAREST-NEIGHBOR DISCRETIZATION OF THE REGULARIZED STOKESLET BOUNDARY INTEGRAL EQUATION*

MEURIG T. GALLAGHER†, DEBAJYOTI CHOUDHURI‡, AND DAVID J. SMITH†

Abstract. The method of regularized stokeslets is a powerful numerical approach to solve the Stokes flow equations for problems in biological fluid mechanics. A recent variation of this method incorporates a nearest-neighbor discretization to improve accuracy and efficiency while maintaining the ease of implementation of the original meshless method. This new method contains three sources of numerical error: the regularization error associated with using the regularized form of the boundary integral equations (with parameter ε), and two sources of discretization error associated with the force and quadrature discretizations (with lengthscales h_f and h_q). A key issue to address is the quadrature error; initial work has not fully explained observed numerical convergence phenomena. In the present manuscript we construct sharp quadrature error bounds for the nearest-neighbor discretization, noting that the error for a single evaluation of the kernel depends on the smallest distance (δ) between these discretization sets. The quadrature error bounds are described for two cases: disjoint sets ($\delta > 0$) that are close to linear in h_q and insensitive to ε, and contained sets ($\delta = 0$) that are quadratic in h_q with inverse dependence on ε. The practical implications of these error bounds are discussed in reference to the condition number of the matrix system for the nearest-neighbor method, with the analysis revealing that the condition number is insensitive to ε for disjoint sets, and grows linearly with ε for contained sets. Error bounds for the general case ($\delta \geq 0$) are revealed to be proportional to the sum of the errors for each case.

Key words. quadrature error bounds, regularized stokeslets, stokes flow, boundary integral equation

AMS subject classifications. 35Q35, 65G99, 65M15, 76D07, 76M25, 76Z05

DOI. 10.1137/18M1191816

1. Introduction.

The development of numerical methods for the solution of Stokes flow has had significant impact on the study of problems in biological fluid dynamics [1, 14, 15, 20, 21, 23] and vice versa. While there have been many powerful methods developed over the past few decades, one of the most effective and accessible tools for solving such problems is the method of regularized stokeslets, conceived of and developed by Cortez and colleagues [2, 7, 8, 9, 10, 11], and recently extended to incorporate the use of the fast multipole method [16]. A key advantage of this method over previous offerings is the meshless nature of implementation, saving the significant investment of time and effort required to generate a mesh (particularly when dealing with complex biomolecular or cellular structures), with the potential to aid automation for applications in image analysis. These methods have had significant impact on a wide-ranging set of applications; a Google Scholar search on September 27, 2018 for the term "regularized stokeslets" yields approximately 40 to 50 results per year over the past five years.

A new variation on the method of regularized stokeslets was recently proposed by

*Submitted to the journal's Computational Methods in Science and Engineering section June 1, 2018; accepted for publication (in revised form) November 5, 2018; published electronically February 19, 2019.

http://www.siam.org/journals/sisc/41-1/M119181.html

Funding: This work was supported by Engineering and Physical Sciences Research Council award EP/N021096/1.

†School of Mathematics, University of Birmingham, Edgbaston, West Midlands, B15 2TT, UK (m.t.gallagher@bham.ac.uk, d.j.smith@bham.ac.uk).

‡Department of Mathematics, NIT Rourkela, Rourkela, 769 008, India (choudhurid@nitrkl.ac.in).

Smith [18], who uses a nearest-neighbor discretization of the regularized stokeslet boundary integral equation to improve the accuracy and efficiency of the classic Nyström discretization [8] while retaining the advantages of a meshless method. The computational efficiency of this new method, together with its extension to problems of locomotion in Stokes flow [12], enables the study of previously computationally intractable problems such as improving the detailed modelling of the embryonic node of mice and zebrafish to incorporate Brownian and other effects, thus improving physiological accuracy.

Mathematical details of the nearest-neighbor discretization will be provided in subsection 1.1. For now we note that the sources of error for the method are threefold: the regularization error associated with using a regularized form of the boundary integral equations (with regularization parameter ε), and two sources of discretization error associated with approximating the integral of the kernel at quadrature points with fine discretization lengthscale h_q, and with approximating the forces with coarser discretization lengthscale h_f. While the original paper of Smith [18] provided an initial estimate of the error for the nearest-neighbor method in terms of these two discretization lengthscales and the regularization parameter, these error bounds were noted not to be sharp, as they did not fully replicate the sensitivity to ε suggested by the analysis (and seen in the classic Nyström discretization).

The relationship between the regularization parameter ε and the error, as well as finding ways of reducing this dependence, have been of key concern to several authors working with regularized stokeslet methods. Noting that the value of ε has the most significant impact when evaluating the regularized stokeslet $S^{\varepsilon}(\boldsymbol{x}, \boldsymbol{y})$ at $\boldsymbol{x} = \boldsymbol{y}$, Barrero-Gil [3] proposed introducing a dense patch of "auxiliary stokeslets" about such points and observing the averaged value of S^{ε} over these patches. By then requiring ε to be equal to this fine discretization lengthscale, Barrero-Gil demonstrated a reduced number of kernel operations when compared to the Nyström discretization, as well as a weakened dependence on the regularization parameter ε. The present method involving a pair of grids is simple to implement, and we will compare its efficiency and accuracy with the method of Barrero-Gil in section 5.4.

There have been many excellent recent works on reducing quadrature errors and creating high-accuracy methods for solving the boundary integral equations (see, for example, [5, 22, 20, 1, 6, 19]). The nearest-neighbor method does not aim to compete with these relatively more complex approaches for accuracy. Instead the objective is to strike a balance between accuracy, efficiency, and ease of use, the latter specifically through avoiding the need to generate a smooth surface geometry or "mesh." The present method has a significantly reduced error compared to the classical (Nyström) discretization, while retaining a simplicity which enables its implementation by non-experts for the investigation of many biologically relevant problems in Stokes flow. Indeed we argue that the major interest in regularized stokeslet methods among the biological fluid mechanics community over the past decade is largely because of its ease of use.

In the present work we not only provide the detailed analysis for calculating sharp error bounds for the nearest-neighbor discretization (section 2), in doing this we uncover why the original work did not see the dependence on the regularization parameter ε and detail the situations where this dependence exists. We then also consider how these errors scale up in solving a practical problems (section 3). Each of these analyses are then confirmed with numerical experiments (section 4). These results will provide clear guidance for the best choices of discretization lengthscales and regularization parameter for given computational scenarios.

1.1. Mathematical background. The dimensionless form of the Stokes flow equations, which describe the very low Reynolds number fluid dynamics associated with sperm and cilia, is given by

$$-\boldsymbol{\nabla} p + \nabla^2 \boldsymbol{u} = 0, \quad \nabla \cdot \boldsymbol{u} = 0, \tag{1.1}$$

augmented with the no-slip, no-penetration boundary condition $\boldsymbol{u}(\boldsymbol{X}) = \dot{\boldsymbol{X}}$ for boundary points $\boldsymbol{X}$, where the overdot denotes time-derivative.

Regularized stokeslet methods involve representing the flow field around a body B by an integral of the form

$$u_j(\boldsymbol{x}) = -\frac{1}{8\pi} \iint_B S^{\varepsilon}_{jk}(\boldsymbol{x}, \boldsymbol{y}) f_k(\boldsymbol{y}) dS_{\boldsymbol{y}}, \tag{1.2}$$

where S^{ε}_{jk} is the velocity part of the solution to the Stokes flow equations (1.1) driven by a smoothed point force in the k-direction, with regularization parameter $\varepsilon > 0$. The most widely-studied example [8] is for three-dimensional (3D) flow and takes the form

$$S^{\varepsilon}_{ij}(\boldsymbol{x}, \boldsymbol{y}) = \delta_{ij} \frac{|\boldsymbol{x} - \boldsymbol{y}|^2 + 2\varepsilon^2}{(|\boldsymbol{x} - \boldsymbol{y}|^2 + \varepsilon^2)^{3/2}} + \frac{(x_i - y_i)(x_j - y_j)}{(|\boldsymbol{x} - \boldsymbol{y}|^2 + \varepsilon^2)^{3/2}}. \tag{1.3}$$

The limiting form of this kernel is the classical stokeslet or Oseen tensor,

$$S_{jk}(\boldsymbol{x}, \boldsymbol{y}) = \frac{\delta_{jk}}{|\boldsymbol{x} - \boldsymbol{y}|} + \frac{(x_j - y_j)(x_k - y_k)}{|\boldsymbol{x} - \boldsymbol{y}|^3}. \tag{1.4}$$

Regularized stokeslet methods are implemented numerically by imposing (1.2) for $\boldsymbol{x} = \boldsymbol{X} \in B$ together with the condition $\boldsymbol{u}(\boldsymbol{X}) = \dot{\boldsymbol{X}}$ (collocation), followed by discretization of the unknown traction $\boldsymbol{f}(\boldsymbol{y})$ and the numerical quadrature. The original (Nyström) discretization of (1.2), by Cortez, Fauci, and Medovikov [8], takes the form

$$u_j(\boldsymbol{X}[m]) = \frac{1}{8\pi} \sum_{q=1}^{Q} S^{\varepsilon}_{jk}(\boldsymbol{X}[m], \boldsymbol{X}[q]) F_k[q], \tag{1.5}$$

where $\{\boldsymbol{X}[1], \ldots, \boldsymbol{X}[Q] \in B\}$ is a set of quadrature points, and the discretized force at $\boldsymbol{X}[q]$ is written as $F_k[q] = -f_k(\boldsymbol{X}[q]) dS(\boldsymbol{X}[q])$. This method has the major advantage of implementational simplicity, a property which has resulted in its widespread adoption; caveats are that the regularization parameter ε and discretization size h must be chosen in proportion, and that the typical size of the linear system ($3Q \times 3Q$) may be much larger than would be required by a classical boundary integral method to achieve converged results. This scaling then limits the applications of the method when considering large or complex problems.

The constant-panel boundary element discretization suggested by Smith [17] takes the form

$$u_j(\boldsymbol{x}[m]) = \frac{1}{8\pi} \sum_{n=1}^{N} f_k[n] \iint_{B_n} S^{\varepsilon}_{jk}(\boldsymbol{x}[m], \boldsymbol{y}) dS_{\boldsymbol{y}}, \tag{1.6}$$

where $\{B_1, \ldots, B_N\}$ is a partitioning of the surface B (mesh) with centroids $\boldsymbol{x}[n] \in B_n$, and the discretization of the traction on B_n is denoted $f_k[n]$. Because the near-field

of the regularized stokeslet is rapidly-varying (resembling the function $(r^2+\varepsilon^2)^{-1/2}$ as $r \to 0$), this traction discretization need not be as refined as the quadrature discretization in (1.5), i.e., one can take $N \ll Q$. The stokeslet integral in (1.6) is still evaluated numerically via quadrature. However, in contrast to (1.5), the quadrature discretization does not affect the number of degrees of freedom of the resulting linear system. The boundary element discretization is therefore more efficient and accurate than the Nyström method; however, it has the disadvantage of requiring true mesh generation rather than a simple list of surface points.

To attempt to combine the implementational simplicity of the Nyström method with the efficiency and accuracy of the boundary element discretization, Smith [18] proposed the use of a meshless nearest-neighbor method. Two discretizations are generated, a "coarse force" set $\mathcal{F} = \{\boldsymbol{x}[1], \ldots, \boldsymbol{x}[N]\}$ and a "fine quadrature" set $\mathcal{Q} = \{\boldsymbol{X}[1], \ldots, \boldsymbol{X}[Q]\}$, with $N < Q$. The force at the quadrature points $\boldsymbol{f}(\boldsymbol{y})dS(\boldsymbol{X}[q])$ is approximated by its value at the nearest force point via a nearest-neighbor interpolation denoted $\mathcal{N} : \{1, \ldots, Q\} \to \{1, \ldots, N\}$. The nearest-neighbor operator can be expressed by the binary matrix

$$\nu[q,n] = \begin{cases} 1 & \text{if } n = \underset{\hat{n}=1,\ldots,N}{\operatorname{argmin}} |\boldsymbol{x}[\hat{n}] - \boldsymbol{X}[q]|, \\ 0 & \text{otherwise.} \end{cases} \tag{1.7}$$

Using this discretisation the regularized stokeslet boundary integral (1.2) can be approximated by the quadrature rule

$$\begin{aligned} -\iint_B S^{\varepsilon}_{jk}(\boldsymbol{x},\boldsymbol{y}) f_k(\boldsymbol{y}) dS_{\boldsymbol{y}} &\approx \sum_{q=1}^{Q} S^{\varepsilon}_{ij}(\boldsymbol{x}, \boldsymbol{X}[q]) f_j(\boldsymbol{X}[q]) dS(\boldsymbol{X}[q]) \\ &\approx \sum_{q=1}^{Q} S^{\varepsilon}_{ij}(\boldsymbol{x}, \boldsymbol{X}[q]) \sum_{n=1}^{N} \nu[q,n] f_j(\boldsymbol{x}[n]) dS(\boldsymbol{x}[n]), \end{aligned} \tag{1.8}$$

resulting in the linear system

$$u_j(\boldsymbol{x}[m]) = \frac{1}{8\pi} \sum_{n=1}^{N} \left(\sum_{q=1}^{Q} S^{\varepsilon}_{jk}(\boldsymbol{x}[m], \boldsymbol{X}[q]) \nu[q,n] \right) F_k[n], \tag{1.9}$$

where $\boldsymbol{F}[n] = \boldsymbol{f}(\boldsymbol{x}[n])dS(\boldsymbol{x}[n])$. We note here that, as with the traction, the weights $dS(\boldsymbol{x}[n])$ vary much more slowly than the stokeslets, motivating the form of (1.9).

Smith [18] conducted an initial analysis of the error associated with the nearest-neighbor method (1.9). In addition to a regularization error $O(\varepsilon)$ found by Cortez, Fauci, and Medovikov [8], the error associated with discretization of the traction is $O(h_f)$ (where h_f characterizes the fineness of the force points), and the error associated with numerical quadrature was estimated to be $O(\varepsilon^{-2} h_f^2 h_q) + O(h_f^{-1} h_q)$, where h_q characterizes the fineness of the quadrature points; formal definitions found in (2.2) and (2.3). It was noted that this error bound was not sharp because numerical experiments suggested that the error does not diverge for very small values of ε. Indeed, the choice of h_f as the lengthscale for quadrature discretization error was somewhat arbitrary. In the present manuscript we will address this issue further. It will be shown that the quadrature error for a single evaluation of the kernel depends on the shortest distance from the force discretization ($\mathcal{F}$) to the quadrature discretization ($\mathcal{Q}$), denoted by δ. The error of the full problem is then discussed in terms of three

FIG. 1. *Schematic detailing of the characterizations for potential force ($\mathcal{F}$) and quadrature ($\mathcal{Q}$) discretization sets with δ, denoting the minimum distance between the discretizations, defined in* (2.1). *Each choice is further shown as belonging to either the set of nearest-neighbor or classic (Nyström) discretizations.*

distinct cases (detailed in Figure 1): (i) when $\delta > 0$, i.e., the force and quadrature sets are disjoint, (ii) when $\delta = 0$, i.e., every force point is also a quadrature point, and (iii) when the force and quadrature sets are nondisjoint, but $\delta = 0$ for some points.

2. Analysis of the quadrature error for a single kernel evaluation. The principal challenge regarding numerical quadrature concerns evaluation where the kernel is rapidly-varying, i.e., where $|\boldsymbol{x}-\boldsymbol{y}|$ is "small." For the Nyström discretization the near-field part of the integral is primarily evaluated in the sum (1.5) when $q = m$. It is clear that this evaluation is problematic as $\varepsilon \to 0$ because $S^{\varepsilon}_{jk}(\boldsymbol{x}, \boldsymbol{x}) \to \varepsilon^{-1}$ as $\varepsilon \to 0$. This divergence also underlies the $O(\varepsilon^{-2} h_f^2 h_q)$ term in the nearest-neighbor error estimate. A key advantage of the nearest-neighbor method, however, is that this situation can be avoided by ensuring that the force and quadrature discretizations are disjoint. We will denote the minimum distance between the discretizations by

$$\delta = \min_{q=1,\ldots,Q} \min_{n=1,\ldots,N} |\boldsymbol{x}[n] - \boldsymbol{X}[q]|. \tag{2.1}$$

If any overlap $\boldsymbol{x}[n] = \boldsymbol{X}[q]$ occurs, then clearly $\delta = 0$. We also recall from [18] the definitions characterizing the fineness of the force and quadrature discretizations,

$$h_f = \max_{m=1,\ldots,N} \min_{n=1,\ldots,N; n\neq m} |\boldsymbol{x}[m] - \boldsymbol{x}[n]|, \tag{2.2}$$

$$h_q = \max_{p=1,\ldots,Q} \min_{q=1,\ldots,Q; q\neq p} |\boldsymbol{X}[p] - \boldsymbol{X}[q]|. \tag{2.3}$$

We note then that we can characterize the choices of force ($\mathcal{F}$) and quadrature ($\mathcal{Q}$) discretizations for the nearest-neighbor method as one of three possibilities:

1. *Disjoint*, $\mathcal{F} \cap \mathcal{Q} = \varnothing$ $(\delta > 0)$.
2. *Contained*, $\mathcal{F} \subset \mathcal{Q}$ $(\delta = 0)$.
3. *General*, $\mathcal{F} \cap \mathcal{Q} \neq \varnothing$ with $\mathcal{F} \not\subset \mathcal{Q}$ $(\delta \geq 0)$.

These cases are illustrated in the schematic provided in Figure 1, with the classic (Nyström) discretization (which has $\delta = 0$) included for comparison.

We will develop detailed analyses of the quadrature error of, in order, the disjoint case (subsection 2.2) and the contained case (subsection 2.3). These will be based on analysis of the error of approximation of $\int_0^{2\pi} \int_0^1 K(r) r dr d\theta$, where $K(r) = (r^2 + \varepsilon^2)^{-1/2}$, which captures the near-singular behavior of the kernel $S^{\varepsilon}_{jk}(\boldsymbol{x}, \boldsymbol{y})$ for small $|\boldsymbol{x} - \boldsymbol{y}|$. In section 3 we will discuss how the quadrature errors scale for practical problems and explore the general case of mixed disjoint and contained quadrature sets.

2.1. Previous analysis. As discussed by Smith [18], an estimate of quadrature error can be made using the mean value inequality $|K(r) - K(0)| \leqslant M_1 r$, where M_1 is a bound on $|K'(r)|$. Because $K'(r) = -r(r^2 + \varepsilon^2)^{-3/2}$, we have for all constants $a > \varepsilon$:

1. In the region $0 \leqslant r \leqslant a$, the bound $M_1 = O(\varepsilon^{-2})$.
2. In the region $a \leqslant r$, the bound $M_1 = |K'(a)|$.

Smith [18] used the above to split the quadrature into three regions, (i) $0 < r < h_f$, (ii) $h_f < r < h_f^{1/2}$, and (iii) $h_f^{1/2} < r < 1$. The quadrature errors can be estimated from the values of M_1, the area of the region, and the quadrature spacing. The resulting error estimates, for each region in turn, are then (i) $O(\varepsilon^{-2} h_f^2 h_q)$, (ii) $O(h_f^{-1} h_q)$, and (iii) $O(h_f^{-1} h_q)$.

2.2. The disjoint case. To expand upon this analysis we first address the case for which $\delta > 0$. This entails that there is an inner region $0 \leqslant r < \delta$ which contains no quadrature points, i.e., the region is neglected from the numerical quadrature. The error associated with this neglect can be calculated as

$$L(\delta, \varepsilon) = \int_0^{2\pi} \int_0^{\delta} K(r) r dr d\theta = 2\pi \left[(\delta^2 + \varepsilon^2)^{1/2} - \varepsilon \right] = O(\delta). \tag{2.4}$$

This error estimate is valid provided $0 < \delta, \varepsilon \ll 1$ regardless of the relative sizes of ε and δ.

The remaining error can be calculated by an approach similar to subsection 2.1. To achieve a sharp error estimate, we will consider a sequence of annuli $\delta \leqslant r < h_q^{\phi_1}$, $h_q^{\phi_1} \leqslant r < h_q^{\phi_2}, \ldots$, where $\phi_1 = 1$ and $\phi_1 > \phi_2 > \ldots$ (this analysis deals with the case $\delta < h_q$; if $\delta \geqslant h_q$ the error is no worse). The quadrature error for the first annulus is $\delta^{-2} h_q^{2\phi_1 + 1}$ and for the nth annulus is $O(h_q^{2(\phi_n - \phi_{n-1}) + 1})$.

Therefore, it is clear that taking $\phi_n - \phi_{n-1}$ to be small and negative will yield a close-to-optimal error estimate. For example, for any fixed integer $P > 3$ we may take $\phi_n = 1 - (n-1)/P$ for $n = 1, \ldots, P+1$. The error for the first annulus is $O(\delta^{-2} h_q^3) = O((h_q/\delta)^2 h_q)$, and for the remaining annuli is $O(h_q^{1-2/P})$. The total error over P annuli is therefore $O((h_q/\delta)^2 h_q) + O(P h_q^{1-2/P})$. By taking increasingly large values of P, the latter term approaches linear convergence. Therefore, provided $h_q/\delta = O(1)$, quadrature convergence is linear in h_q and insensitive to ε.

In summary, the total error estimate (including regularization error, force discretization error, and quadrature error) for the nearest-neighbor regularized stokeslet method with disjoint discretizations is

$$E_1 = O(\varepsilon) + O(h_f) + O((h_q/\delta)^2 h_q) + O(P h_q^{1-2/P}) \tag{2.5}$$

for any integer $P > 3$, where δ is the minimum distance from the force discretization to the quadrature discretization, as defined in (2.1).

2.3. The contained case. The analysis of subsection 2.1 is based on three regions parameterized by h_f. The argument is, in fact, valid with h_f replaced by any lengthscale $\lambda > \varepsilon/\sqrt{2}$ so that the local maximum of $|K'(r)|$ appears inside the inner circle $0 \leqslant r < \lambda$. By arguments similar to the above (based on taking annuli of radius $\lambda^{1-(n-1)/P}$) we then have the total error estimate

$$O(\varepsilon) + O(h_f) + O(\varepsilon^{-2} \lambda^2 h_q) + O(P \lambda^{-2/P} h_q). \tag{2.6}$$

Taking $\lambda = \varepsilon^{1/2} h_q^{1/2}$ yields an error

$$E_2 = O(\varepsilon) + O(h_f) + O(\varepsilon^{-1} h_q^2) + O(P \varepsilon^{-1/P} h_q^{1-1/P}). \tag{2.7}$$

As $\varepsilon \to 0$, the dominant term in the above is $O(\varepsilon^{-1} h_q^2)$, which has the very advantageous property of being quadratic in h_q, but an unwanted inverse dependence on ε. It is, therefore, clear for the contained case that we cannot expect it to be able to reduce ε independently of h_q.

3. Practical implications of the quadrature error. Having developed the analysis to understand the quadrature error inherent in a single evaluation of the kernel, it is of practical use to assess how this error scales in a full application of the nearest-neighbor discretization (when solving a resistance problem, for example). When numerically constructing and solving the matrix system $A\boldsymbol{\chi} = \boldsymbol{b}$ the relative error in the calculation of $\boldsymbol{\chi}$ in terms of small deviations in the construction of matrix A, ΔA, is bounded by

$$\left\| \frac{\Delta \boldsymbol{\chi}}{\boldsymbol{\chi}} \right\| \leq \left\| A^{-1} \right\| \|A\| \frac{\|\Delta A\|}{\|A\|} = \operatorname{cond}(A) \frac{\|\Delta A\|}{\|A\|}, \tag{3.1}$$

where $\operatorname{cond}(A)$ represents the condition number of A, and $\|\Delta A\|/\|A\|$ is the relative error in the numerical construction of A. The analysis of section 2 provides the error estimates for the size of $\|\Delta A\|/\|A\|$ for both disjoint (subsection 2.2) and contained (subsection 2.3) quadrature sets; to build an understanding of the error in a practical application of the nearest-neighbor method it thus remains to understand how the condition number of the matrix A behaves.

Each row of the matrix A consists of a diagonal entry which comes from evaluation of S_{ij}^{ε} (1.3) at the force and associated nearest-neighbor quadrature points. Consequently, for numerically tractable numbers of quadrature points Q, the diagonal entries of A have lower bound,

$$A_{ii} \geq \overline{A} \propto \begin{cases} \left(\delta^2 + \varepsilon^2\right)^{-1/2} & \text{for a disjoint quadrature set,} \\ \varepsilon^{-1} & \text{for a contained quadrature set.} \end{cases} \tag{3.2}$$

In the case when Q becomes large, then the change in the diagonal entries of A due to the evaluation of S_{ij}^{ε} at many points will become significant; we will explore this numerically in section 4. However, for practical densities of quadrature points this source of error is insignificant compared to the dominant (ε^{-1}) term. Denoting the sum of the off-diagonal elements (corresponding to a surface integral over a fixed area) by C_Q, which will grow with increasing numbers of quadrature points Q, we can apply the Gershgorin circle theorem [4] to show that all eigenvalues of A lie in a circle of radius C_Q about the diagonal values in (3.2). The ratio between the largest and smallest eigenvalues (the condition number) is therefore bounded by

$$\frac{1/\varepsilon + C_Q}{1/\varepsilon - C_Q} \sim 1 + 2C_Q\varepsilon \tag{3.3}$$

for a contained quadrature set, and for a disjoint quadrature set, as $\varepsilon \to 0$,

$$\frac{1/\delta_{\min} + C_Q}{1/\delta_{\max} - C_Q} \sim \frac{\delta_{\max}}{\delta_{\min}} \left(1 + C_Q \left(\delta_{\min} + \delta_{\max}\right)\right), \tag{3.4}$$

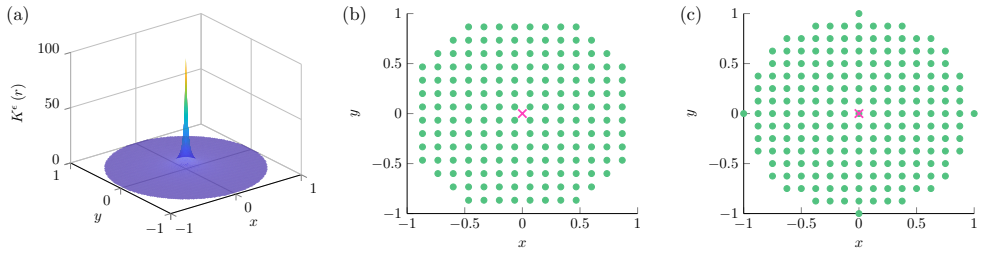

FIG. 2. *Set up for numerical quadrature experiments.* (a) *The near-singular kernel* $K^\varepsilon(r)$ *plotted for* $r < 1$ *with* $\varepsilon = 0.01$. (b) *Depiction of a disjoint quadrature set with* $h_q = 1.33$. (c) *Depiction of an contained quadrature set with* $h_q = 0.125$. *(Figure in color online.)*

where $\delta_{\min}$ and $\delta_{\max}$ are, respectively, the smallest and largest of the distances δ (as calculated in (2.1)) between each force and quadrature discretization sets, with $\delta_{\max} \ll 1$ (and assuming $\delta_{\max}/\delta_{\min} = O(1)$). Provided again that Q is not too large (which will cause C_Q to correspondingly increase), is clear that this method resolves a problem that affects boundary element methods for Stokes flow by ensuring that the condition number remains bounded as the size of the force elements approaches zero.

The bounds that this analysis places on the condition number of the matrix A are practically very useful when solving problems with the nearest-neighbor discretization. There may be situations where it is desirable to discretize a subject with both disjoint and contained quadrature sets; when considering a biological swimmer, for example, it may be helpful to consider separately the discretization of flagellum and body. We can thus consider the error of the *general case* as being composed of the error from the *disjoint case*, E_1 (2.5), plus the error from the *contained case*, E_2 (2.7), multiplied by the condition number of the matrix A.

4. Numerical experiments. We will now confirm the analysis through numerical experiments. Subsection 4.1 will consider the convergence of numerical quadrature of the function $K^\varepsilon(r) = (r^2 + \varepsilon^2)^{-1/2}$ for a region including $r = 0$, subsection 4.2 will investigate the condition number of the matrix A, and subsection 4.3 the resistance tensor, each relating to the problem of a prolate spheroid undergoing rigid body motion.

4.1. Quadrature convergence. The function $K^\varepsilon(r)$ is illustrated in Figure 2a. Two types of quadrature methods are illustrated: disjoint quadrature (Figure 2b) for which the quadrature set does not include the origin, and contained quadrature (Figure 2c) for which the quadrature set does include the origin. Numerical results with these quadrature sets are shown in Figure 3. The disjoint quadrature set (Figure 3a) exhibits approximately linear convergence with h_q and is insensitive to ε, as expected from equation (2.5). The contained quadrature set performs very well for $\varepsilon = 0.001$, exhibiting approximately quadratic convergence, as expected from (2.7). However, as also predicted, the absolute error shows an approximate ε^{-1} dependence, becoming highly inaccurate for $\varepsilon \leqslant 10^{-5}$.

4.2. Condition number. To assess the condition number analysis of section 3 on a relevant problem we follow Smith [18] and construct the matrix A modeled on the resistance problem of a prolate spheroid associated with rigid body motion. In

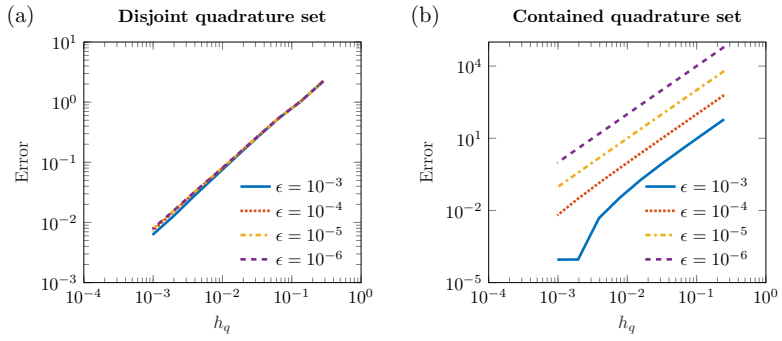

FIG. 3. *Convergence of numerical quadrature of the kernel K^ε with number of points for four values of the regularization parameter ε.* (a) *Disjoint quadrature set.* (b) *Contained quadrature set. (Figure in color online.)*

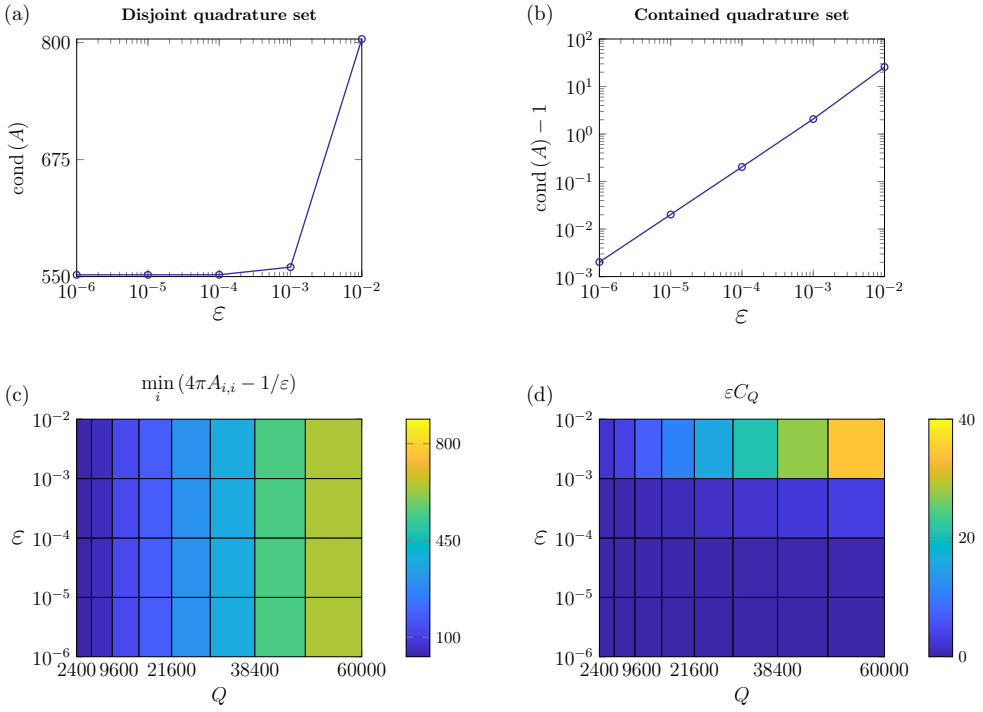

FIG. 4. *Analysis of the condition number and diagonal entries of the matrix A. Panel* (a) *plots the condition number* $\mathrm{cond}\,(A)$ *against ε for a disjoint quadrature set, and shows the robustness of the condition number to changes as $\varepsilon \to 0$. Panel* (b) *plots* $\mathrm{cond}\,(A) - 1$ *against ε for a contained quadrature set, and shows approximate linear dependence with a slope of* 1.02. *Panel* (c) *shows the minimum deviation of the diagonal entries of A away from $1/\varepsilon$ for large numbers of quadrature points Q with a contained quadrature set. Panel* (d) *shows the C_Q, the maximum sum of the off-diagonal entries of A, multiplied by ε for large numbers of quadrature points Q with a contained quadrature set. (Figure in color online.)*

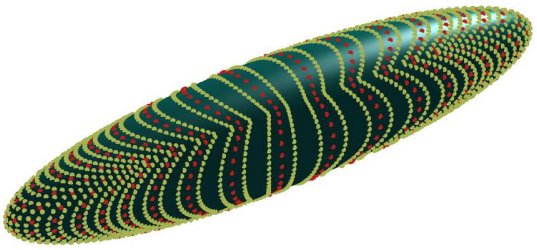

FIG. 5. *Sketch of the nearest-neighbor discretization of a prolate spheroid. Here, the red dots show the force discretization, with a disjoint quadrature set shown in light green. (Figure in color online.)*

Figure 4a we plot the condition number of A against decreasing values of ε for a disjoint quadrature set and, as predicted, we see that the condition number plateaus rapidly as $\varepsilon \to 0$. For a contained quadrature set we plot in Figure 4b $\operatorname{cond}(A) - 1$ against the same values of ε, where we see the approximate linear dependence on this quantity with ε (the slope in the figure is calculated as approximately 1.02). To assess the predictions regarding the diagonal entries of the matrix A, in Figure 4c we plot the minimum increase in diagonal elements of A from $1/\varepsilon$ against increasing numbers of quadrature points Q; here we clearly see that the diagonal terms are indeed bounded with $A_{ii} \geq 1/\varepsilon$. In Figure 4d we plot the maximum row sum of off-diagonal entries C_Q multiplied by ε. Here we see that εC_Q grows slowly with Q; however, for computationally practical values of Q the size of εC_Q (and thus the condition number of A) remain manageable. These numerical results agree with the analysis of section 3, and give us confidence when using the calculated error bounds.

4.3. Resistance problem. To assess the analysis of section 2 on a relevant problem we follow Smith [18] and calculate the resistance tensor of a prolate spheroid, with an axis ratio of 5, associated with rigid body motion. This problem has the added benefit of an analytical solution with which to compare [13]. A rendering of the force and quadrature discretizations for this problem is shown in Figure 5. We again test both disjoint and contained quadrature sets with results provided in Figure 6. The disjoint case again shows approximately linear convergence with $\delta^{-2}h_q^3$ and, if $\varepsilon \leq 10^{-3}$, is very robust to the choice of ε. This robustness is illustrated more clearly in Table 1, which contains a selection of the values used to plot Figure 6a. The contained case exhibits near linear convergence in $\varepsilon^{-1}h_q^2$ for moderate values of ε, and the error collapses onto a single curve. For this case we see, as predicted by the analysis in section 2, a clear dependence on ε, with the relative error approaching 100% for $\varepsilon \leq 10^{-5}$. While we may naively expect the error to blow up for large $\varepsilon^{-1}h_q^2$, the limit of small ε for a contained quadrature set leads to a calculation of zero force, and thus a zero resistance tensor, over the prolate spheroid. This results in a relative error of 100% in the limit $\varepsilon \to 0$.

5. Conclusions. This paper has calculated sharp quadrature error bounds for the nearest-neighbor regularized stokeslet discretization. We have shown that this error depends on the shortest distance (δ) from the force discretization ($\mathcal{F}$) to the quadrature discretization ($\mathcal{Q}$), and that the behavior of the quadrature error can be characterised by two discrete cases. The total error in solving a Stokes flow problem using the nearest-neighbor discretization is described by either of these cases, or by a

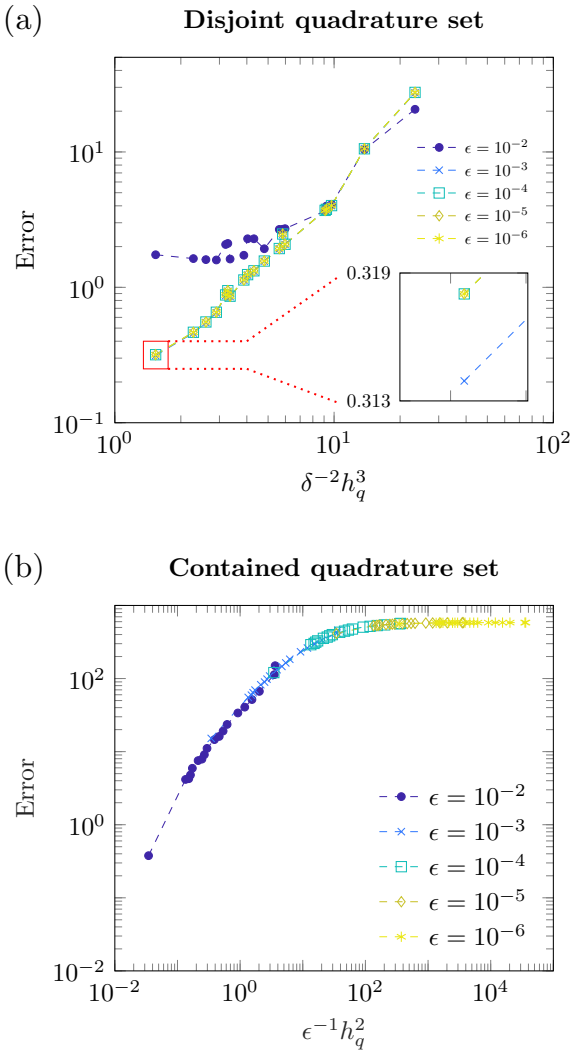

FIG. 6. *Absolute error in calculating the resistance tensor of a prolate spheroid undergoing rigid body motion for* (a) *disjoint and* (b) *contained quadrature sets. In* (a) *we see convergence with decreasing* $\delta^{-2}h_q^3$*, with an insert showing a zoomed view emphasizing the lack of* ε *dependence for* $\varepsilon < 10^{-3}$*. Panel* (b) *shows convergence with decreasing* $\varepsilon^{-1}h_q^2$*. Each panel has been calculated for five values of the regularization parameter* ε *with fixed* $h_f \approx 0.249$*. (Figure in color online.)*

general, mixed case. We will now detail the characteristics of each of these cases in turn.

5.1. The *disjoint* case, $\mathcal{F} \cap \mathcal{Q} = \varnothing$ ($\delta > 0$). When the force and quadrature discretizations are *disjoint*, the total error estimate for the nearest-neighbor regularized stokeslet method is

$$E_1 = O(\varepsilon) + O(h_f) + O\left(\delta^{-2}h_q^3\right) + O\left(Ph_q^{1-2/P}\right)$$

for any integer constant $P > 3$, where $\varepsilon \ll 1$ is the stokeslet regularization parameter, and h_f and h_q are given by (2.2) and (2.3), respectively. In this case the quadrature error is very robust to the choice of ε, with errors that are approximately linear in h_q when $\delta \sim h_q$.

When solving practical problems (of the form $A\boldsymbol{\chi} = \boldsymbol{b}$) with a *disjoint* quadrature set, the condition number of the matrix A is also robust to the choice of ε. This ensures that, provided Q is not too large, the error in solving a practical problem should remain E_1; this error result has been validated through solving the resistance problem of a prolate spheroid undergoing rigid body motion, as displayed in Figure 6a.

For this particular case of *disjoint* force and quadrature sets the regularization error may be eliminated by choosing $\varepsilon = 0$ without affecting the quadrature error (which is equivalent to the implementation of the boundary singularity method; see [14]). However, the advantage of the regularized method (with nonzero ε) is that the calculated flow fields remain regular for many applications.

TABLE 1

Error in calculating the resistance tensor of a prolate spheroid undergoing rigid body motion for a disjoint quadrature set (as depicted in Figure 6a*). The error is calculated for five choices of the regularization parameter ε and increasing $\delta^{-2}h_q^3$, with fixed $h_f \approx 0.249$.*

	$\delta^{-2}h_q^3$						
ε	2.282	3.355	4.805	5.975	9.101	13.75	23.40
10^{-2}	1.603	1.619	1.929	2.712	3.666	10.40	20.66
10^{-3}	0.4600	0.8547	1.560	2.072	3.699	10.55	27.35
10^{-4}	0.4657	0.8602	1.564	2.081	3.702	10.55	27.52
10^{-5}	0.4658	0.8603	1.564	2.081	3.702	10.55	27.52
10^{-6}	0.4658	0.8603	1.564	2.081	3.702	10.55	27.53

5.2. The *contained* case, $\mathcal{F} \subset \mathcal{Q}$ ($\delta = 0$). When the force and quadrature discretizations are *contained*, the total error estimate for the nearest-neighbor regularized stokeslet method is

$$E_2 = O(\varepsilon) + O(h_f) + O\left(\varepsilon^{-1}h_q^2\right) + O\left(P\varepsilon^{-1/P}h_q^{1-1/P}\right)$$

for any integer constant $P > 3$, where $\varepsilon \ll 1$ is the stokeslet regularization parameter, and h_f and h_q are given by (2.2) and (2.3), respectively. In this case the quadrature error is approximately quadratic in h_q, but also has an unwanted inverse dependence of ε. It is clear that in this case we are not able to reduce ε independently of h_q.

When solving practical problems (of the form $A\boldsymbol{\chi} = \boldsymbol{b}$) with a *contained* quadrature set, the condition number of the matrix A grows linearly with ε. This ensures that, provided Q is not too large, the error in solving a practical problem should remain E_2; this error result has been validated through solving the resistance problem of a prolate spheroid undergoing rigid body motion, as displayed in Figure 6b.

The choice of $\varepsilon = h_q$ could therefore provide a good choice for balancing the various error terms specifically for the contained case.

5.3. The *general* case, $\mathcal{F} \not\subset \mathcal{Q}$ ($\delta \geq 0$). We have provided analyses for both the *disjoint* and *contained* cases. It is conceivable that for practical purposes one may wish to use separate discretizations for different elements of a problem (for example, discretizing a swimmer's body and flagella differently), inducing the combination of both disjoint and contained quadrature sets. The analysis of the condition number of

the matrix system indicates that the total error for the solution of practical problems with general force and quadrature sets should be proportional to the sum $E_1 + E_2$.

5.4. Discussion. The analyses were confirmed via numerical experiments: we have tested the convergence of numerical quadrature of the kernel $K^\varepsilon(r)$ (subsection 4.1), assessed the change in condition number of the matrix system (subsection 4.2), and tested the calculation of the resistance tensor of a prolate spheroid undergoing rigid body motion (subsection 4.3). Each of these numerical experiments closely replicated the predictions of the analysis.

The analysis contained within the present work provides useful insight into the error inherent in using the nearest-neighbor discretization; we believe that the application of this analysis when choosing the parameters of the method for a given problem of interest will be valuable in ensuring that the desired convergence criteria are met.

The approach of the nearest-neighbor method reduces degrees of freedom while retaining near field accuracy. For better scaling to large problems involving many far-field evaluations it may be interesting to explore whether fast multipole implementations can be integrated into the nearest-neighbor method. If it is possible for such adaptations to be made while keeping the ease of implementation and simplicity of the present method, then this will surely be valuable. The present method compares favorably with test cases of other methods. Comparison with the method of [3], for the test case of a translating sphere, shows that for a similar number of stokeslet evaluations the present method yields a reduced condition number and a slightly lower relative error (we observe a 15% reduction in relative error in our comparisons).

One area where the nearest-neighbor discretization may prove useful is in the simulation of biological microswimmers. The meshless nature of this method leaves open the possibility for automated swimmer generation from the analysis of experimental imaging data, an option which is far from straightforward for methods which require the generation of a true mesh.

Acknowledgment. The authors would like to thank the anonymous referees for their valuable suggestions.

REFERENCES

[1] L. A. Klinteberg and A.-K. Tornberg, *A fast integral equation method for solid particles in viscous flow using quadrature by expansion*, J. Comput. Phys., 326 (2016), pp. 420–445.
[2] J. Ainley, S. Durkin, R. Embid, P. Boindala, and R. Cortez, *The method of images for regularized Stokeslets*, J. Comput. Phys., 227 (2008), pp. 4600–4616.
[3] A. Barrero-Gil, *Weakening accuracy dependence with the regularization parameter in the method of regularized Stokeslets*, J. Comput. Appl. Math., 237 (2013), pp. 672–679.
[4] H. E. Bell, *Gershgorin's theorem and the zeros of polynomials*, Amer. Math. Monthly, 72 (1965), pp. 292–295.
[5] O. P. Bruno and L. A. Kunyansky, *A fast, high-order algorithm for the solution of surface scattering problems: Basic implementation, tests, and applications*, J. Comput. Phys., 169 (2001), pp. 80–110.
[6] C. Carvalho, S. Khatri, and A. D. Kim, *Asymptotic analysis for close evaluation of layer potentials*, J. Comput. Phys., 355 (2018), pp. 327–341.
[7] R. Cortez, *The method of regularized Stokeslets*, SIAM J. Sci. Comput., 23 (2001), pp. 1204–1225, https://doi.org/10.1137/S106482750038146X.
[8] R. Cortez, L. Fauci, and A. Medovikov, *The method of regularized Stokeslets in three dimensions: Analysis, validation, and application to helical swimming*, Phys. Fluids, 17 (2005), 031504.
[9] R. Cortez and F. Hoffmann, *A fast numerical method for computing doubly-periodic regularized Stokes flow in 3D*, J. Comput. Phys., 258 (2014), pp. 1–14.

[10] R. Cortez and M. Nicholas, *Slender body theory for Stokes flows with regularized forces*, Commun. Appl. Math. Comput. Sci., 7 (2012), pp. 33–62.
[11] R. Cortez and D. Varela, *A general system of images for regularized Stokeslets and other elements near a plane wall*, J. Comput. Phys., 285 (2015), pp. 41–54.
[12] M. T. Gallagher and D. J. Smith, *Meshfree and efficient modeling of swimming cells*, Phys. Rev. Fluids, 3 (2018), 053101.
[13] S. Kim and S. J. Karrila, *Microhydrodynamics: Principles and Selected Applications*, Dover, Mineola, NY, 2013.
[14] C. Pozrikidis, *Boundary Integral and Singularity Methods for Linearized Viscous Flow*, Cambridge University Press, Cambridge, 1992.
[15] C. Pozrikidis, *A Practical Guide to Boundary Element Methods with the Software Library BEMLIB*, Chapman & Hall/CRC, Boca Raton, FL, 2002.
[16] M. W. Rostami and S. D. Olson, *Kernel-independent fast multipole method within the framework of regularized Stokeslets*, J. Fluid. Struct., 67 (2016), pp. 60–84.
[17] D. Smith, *A boundary element regularized Stokeslet method applied to cilia-and flagella-driven flow*, Proc. R. Soc. Lond. A, 465 (2009), pp. 3605–3626.
[18] D. Smith, *A nearest-neighbour discretisation of the regularized Stokeslet boundary integral equation*, J. Comput. Phys., 358 (2018), pp. 88–102.
[19] C. Sorgentone and A.-K. Tornberg, *A highly accurate boundary integral equation method for surfactant-laden drops in* 3*d*, J. Comput. Phys., 360 (2018), pp. 167–191.
[20] S. Veerapaneni, D. Gueyffier, D. Zorin, and G. Biros, *A boundary integral method for simulating the dynamics of inextensible vesicles suspended in a viscous fluid in* 2*D*, J. Comput. Phys., 228 (2009), pp. 2334–2353.
[21] S. Veerapaneni, A. Rahimian, G. Biros, and D. Zorin, *A fast algorithm for simulating vesicle flows in three dimensions*, J. Comput. Phys., 230 (2011), pp. 5610–5634.
[22] L. Ying, G. Biros, and D. Zorin, *A high-order* 3*D boundary integral equation solver for elliptic pdes in smooth domains*, J. Comput. Phys., 219 (2006), pp. 247–275.
[23] A. Zinchenko and R. Davis, *An efficient algorithm for hydrodynamical interaction of many deformable drops*, J. Comput. Phys., 157 (2000), pp. 539–587.